Effects of vacancy defects on thermal conductivity in crystalline silicon: A nonequilibrium molecular dynamics study

Yongjin Lee, Sangheon Lee, and Gyeong S. Hwang[*]

Department of Chemical Engineering, University of Texas, Austin, Texas 78712, USA

(Received 14 September 2010; revised manuscript received 5 December 2010; published 14 March 2011)

We examine the effects of vacancy defects on thermal conductivity in bulk crystalline silicon (c-Si) using nonequilibrium molecular dynamics simulations. While most vacancies are thought to remain in the form of clusters in bulk c-Si, recent theoretical studies have predicted that small vacancy clusters energetically prefer to be fourfold coordinated by nullifying dangling bonds. Hence, in this work, we consider three different-sized fourfold vacancy clusters, tetra- (V_4), hexa- (V_6), and dodeca-vacancy (V_{12}), with particular interest in studying how phonon transport is affected by vacancy concentration and cluster size in association with fourfold coordination-induced lattice distortions. Our simulations show that thermal conductivity (κ) rapidly drops with vacancy concentration (n_v) with an inverse power-law relation ($\kappa \propto n_v^{-\alpha}$, with $\alpha \approx 0.7$–1.1 depending on cluster size); the presence of 1.5% vacancies leads to a 95% reduction in κ as compared to the defect free c-Si. When n_v is low ($<1\%$), the reduction of κ with n_v appears to be a function of cluster size, and the size effect becomes unimportant as n_v increases above 1%. We discuss the correlation between phone scattering and cluster size, based on the relative rates of phonon-vacancy scattering associated with defect-induced strain fields. We also estimate the dependence of phonon mean free path on vacancy concentration and cluster size.

PACS number(s): 65.40.−b

I. INTRODUCTION

With the ever-growing demand for renewable energy, there has been great interest in thermoelectric energy conversion that turns waste heat into electrical energy.[1–4] In addition, thermoelectric cooling appears to be a promising approach for thermal management in small electronic and optoelectronic systems,[5–7] and the technology can be useful for temperature control of satellites and space probes.[8] The efficiency of thermoelectric devices is measured by the figure of merit (ZT), which is defined in dimensionless form as $ZT = S^2\sigma T/\kappa$, where T is the absolute temperature, S the Seebeck coefficient, and σ and κ refer to the electrical conductivity and the thermal conductivity, respectively.[9] Over the past few years, significant improvements in thermoelectric efficiency have been made by mostly lowering thermal conductivity, yet thermoelectrics are still too expensive and inefficient to compete with conventional power generators.

Recently there have been several attempts to utilize Si-based materials, while compound semiconductors have been widely used for thermoelectrics.[10–12] Si is more abundant, safer, and cheaper than compound semiconductors and also has well-established low-cost process technology, making it attractive for thermoelectric applications. However, bulk c-Si is well known to be inefficient as a thermoelectric material because of its high κ; the ZT value of bulk c-Si is on the order of 0.01 at room temperature.[13] Recent studies[1,2,14–16] have evidenced that Si nanopore and nanowire structures exhibit a drastic reduction in κ, thereby leading to enhanced ZT values. In addition, the lattice thermal conductivity of semiconductors can be reduced in the presence of vacancy defects[17–21]; however detailed quantitative analysis of the defect effect in c-Si has not yet been reported.

In this work, we investigate how the presence of vacancy defects affects the thermal conductivity in c-Si using nonequilibrium molecular dynamics simulations. In bulk c-Si, mono- and divacancies are likely mobile even at room temperature,[22,23] and thus most vacancies have been thought to remain in the form of clusters or complexes with other defects and impurities. According to very recent theoretical studies,[24,25] small vacancy clusters (V_n, $3 \leqslant n \leqslant 48$) tend to be fourfold coordinated by nullifying dangling bonds created by Si lattice atom removal; in this size regime, the bond energy gain by fourfold coordination is predicted to exceed the strain energy increase via consequent lattice distortions. Unlike pointlike defects, phonon scattering due to vacancy clusters would be a function of not only vacancy concentration but also cluster size.[26] Particularly, the fourfold coordination of vacancy defects can cause significant lattice distortions around them, which could play an important role in impeding phonon transport. The present study intends to examine the role played by fourfold vacancy clusters in scattering of high-frequency acoustic phonons in bulk c-Si, particularly the concentration and size effects, using three different-sized clusters (V_4, V_6, and V_{12} as illustrated in Fig. 1). The fundamental findings obtained from this paper will assist in better understanding the influence of vacancy defects on Si thermal conductivity, which would be necessary to achieve enhanced thermoelectric properties through defect engineering.

II. COMPUTATIONAL METHODS

Thermal conductivity that refers to the ability of matter to conduct heat is given, according to Fourier's law, by $J = -\kappa dT/dz$, where J is the steady-state heat flux and dT/dz is the temperature gradient. Classical molecular dynamics simulations have been widely employed to estimate the thermal conductivity of semiconductor materials. Nonequilibrium molecular dynamics (NEMD),[27–29] also called the direct method, is analogous to an experimental procedure, in which the heat flux (or temperature gradient) is calculated from the imposed temperature gradient (or heat flux). Equilibrium molecular dynamics (EMD) with the popular Green-Kubo

method[17,30,31] relates heat current fluctuations to κ based on the fluctuation-dissipation theorem.[32] The Green-Kubo approach generally requires a higher computational cost than NEMD, which tends to be its major drawback.

(a) Nonequilibrium molecular dynamics. In this paper, we used NEMD where the temperature gradient was obtained from the imposed heat flux. In the NEMD simulations, we employed the Tersoff bond-order potential[33] for tetrahedrally bonded Si, as implemented in the large-scale atomic/molecular massively parallel simulator (LAMMPS).[34] To induce heat flow, we define a heat sink and a heat source in each simulation cell. The velocity vectors of the hottest atom in the heat sink and the coldest atom in the heat source are interchanged (if the hottest atom has a higher kinetic energy than the coldest atom). The unphysical energy transfer (from the cold region to the hot region) leads to a heat flow in the opposite direction by thermal conduction. At steady state, both fluxes are equal in magnitude, and the total heat flux is obtained from the sum of the kinetic energies transferred. As such, the thermal conductivity (κ) of a given system is then calculated by

$$\kappa = -\frac{J}{(dT/dz)} = -\frac{\sum_{\text{swaps}}(m/2)\left(v_{\text{hot}}^2 - v_{\text{cold}}^2\right)}{2t\,A(dT/dz)}, \qquad (1)$$

where v_{hot} and v_{cold} refer to the velocities of the atoms involved in the energy exchange in the cold and hot segments, respectively, t is the simulation time, A is the cross-sectional area perpendicular to the heat-flow direction, and dT/dz is the temperature gradient in the longitudinal direction (z direction). The factor of 2 in the denominator indicates that heat flows in two directions due to the periodic boundary condition imposed in the z direction (see Fig. 2).

(b) Simulation cell construction. As model defects, we adopted stable fourfold-coordinated tetra- (V_4), hexa- (V_6), and dodeca-vacancy (V_{12}) clusters from the previous work of Lee and Hwang[24]; the predicted lowest-energy configurations of the vacancy clusters are shown in Fig. 1. The fourfold-coordinated structures remained stable during MD simulations at 300 K, which is not surprising considering that all Si atoms are fourfold coordinated with no significant distortions. The predicted formation energies (per vacancy) of 2.04, 1.53, and 1.15 eV using the Tersoff potential are close to the density functional theory (DFT) values of 1.88, 1.62, and 1.16 eV for V_4, V_6, and V_{12}, respectively. This implies that the empirical potential can describe reasonably well the structure and energetics of fourfold-coordinated vacancy defects where the bond lengths and bond angles insignificantly deviate from their equilibrium values.

For each simulation cell, V_4, V_6, or V_{12} clusters at a given concentration were randomly embedded in the middle layers, which are separated from the heat sink and source layers by 5.4313-nm-thick buffer layers, as illustrated in Fig. 2. As such, the periodic simulation cell consists of heat source and sink layers (indicated as S_H and S_C, respectively), two vacancy-embedded intermediate (I) layers, and two buffer (B) layers. Because there is velocity switching-induced nonphysical phonon scattering in the heat source and heat sink segments,[35,36] it might be necessary to place vacancy defects outside those regions to better assess phonon transport in the defective structures without the unphysical scattering
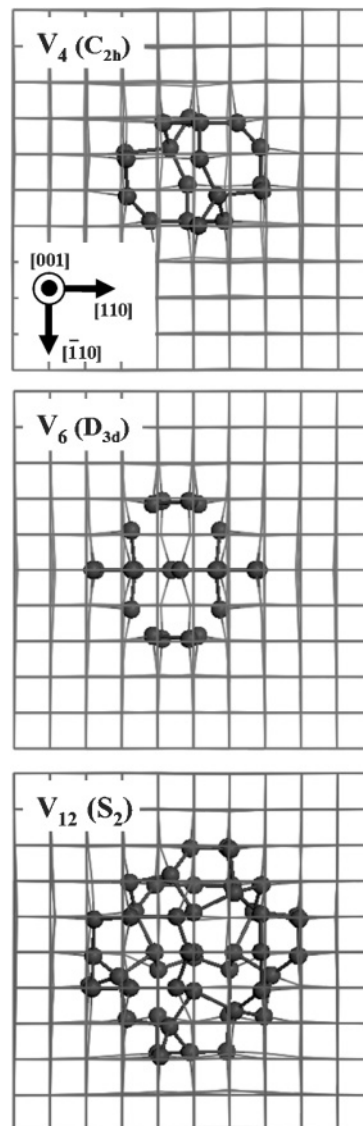

FIG. 1. Minimum energy configurations of fourfold tetra- (V_4), hexa- (V_6), and dodeca-vacancy (V_{12}) clusters considered in this paper. Wire frame represents the bulk Si lattice, and spheres represent highly strained atoms due to the fourfold coordination of the neighboring atoms around the vacancies.

contribution. In addition, we assured that linear temperature gradients were established in the vacancy-embedded layers by adjusting the length of buffer layers (in which temperature profiles were frequently highly nonlinear).

For all simulation cells, fixed lattice constants of 5.4313 Å along $\langle 100 \rangle$ and 3.8405 Å along $\langle 110 \rangle$ were used for c-Si, as obtained from volume optimization with the Tersoff potential. The cross section of each simulation cell consists of 10×10 units (corresponding to 3.8405×3.8405 nm^2 or 400 atoms). The thickness of the heat source and heat sink layers is $L_S = 5.4313$ Å (corresponding to one unit in the axial direction or 400 atoms), and the each buffer layer thickness is set to $L_B = 54.313$ Å (corresponding to 10 units or 4000 atoms). The axial length of the vacancy-embedded intermediate layer varies from $L_I = 21.7252$, 43.4504, and 65.1756 to 86.9008 nm (corresponding to 40, 80, 120, and 160
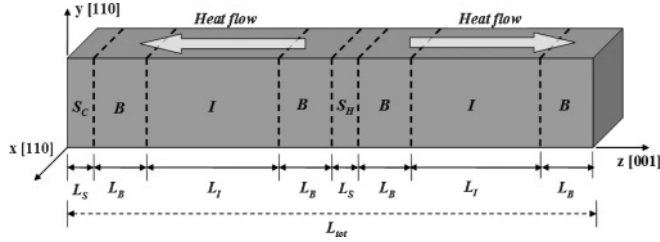
FIG. 2. Schematic illustration of the three-dimensional periodic simulation cell that consists of heat source (S_H), heat ink (S_C), buffer (B), and intermediate (I) layers; corresponding layer thicknesses (L_S, L_B, L_I) are also shown. Vacancy clusters are randomly embedded only in the intermediate (I) layers to avoid the influence of velocity switching-induced nonphysical phonon scattering in the heat source and sink regions. Heat flows in two directions due to the periodic boundary condition imposed in the $\langle 100 \rangle$ direction, as indicated.

units, respectively, in the $\langle 100 \rangle$ direction). Periodic boundary conditions are imposed in the x, y, and z directions, while heat conduction occurs in the z direction.

(c) NEMD determination and quantum correction of k. For each system, we performed ten independent NEMD simulations with different initial velocity distributions; the system was initially equilibrated at 300 K within the *NVT* ensemble with a Nosé-Hoover thermostat for 100 picoseconds (ps), followed by 2000 ps of constant energy (*NVE*) MD while imposing a heat flux and measuring the ensuing temperature gradient. A time step of 1 femtosecond (fs) was adopted for all MD simulations reported herein. Here, care should be taken that the frequency of velocity swaps is such that the temperature profiles of the system are linear in the intermediate regions, so as to obey Fourier's law. A lower swapping frequency, or a smaller heat flux, may be preferable, but a higher swapping frequency may lead to faster equilibration and in turn improved computational efficiency. Several careful test runs showed that a swap interval of once every 100 MD steps can be sufficient to provide reasonable results for all cases examined. In our simulations, each temperature profile was obtained by averaging over 10^5 MD steps (100 ps) after equilibrium was reached.

In the MD approach, the temperature is commonly calculated from the velocities of constituent atoms based on the equipartition theorem of classical statistical mechanics, $\frac{3}{2} N k_B T_{\text{MD}} = \frac{1}{2} \sum_{i=1}^N m v_i^2$, where N is the number of atoms in a chosen region (one unit or shell here), k_B is the Boltzmann constant, v_i is the velocity of atom i, and m is the atomic mass. However, because the system temperature of 300 K is below the Si Debye temperature (=645 K),[37] quantum corrections to the MD temperature (T_{MD}) and thermal conductivity (κ_{MD}) are necessary. By assuming that the total system energy is the mean kinetic energy at T_{MD} and equals the total phonon energy at a quantum temperature T, the quantum correction can be $\langle E \rangle = 3 N k_B T_{\text{MD}} = \int_0^{\omega_D} D(\omega)(\frac{1}{2} + \frac{1}{\exp(\hbar\omega/k_B T)-1})\hbar\omega \, d\omega$, where $D(\omega)$ is the phonon density of states for all acoustic branches, ω is the phonon frequency, and the 1/2 in the phonon energy term represents the effect of zero-point energy. Here, the phonon occupation number is described in terms of the Planck distribution function ($\frac{1}{\exp(\hbar\omega/k_B T)-1}$). From $J = -\kappa_{\text{MD}} \frac{dT_{\text{MD}}}{dz} = -\kappa \frac{dT}{dz}$, the corrected thermal conductivity

is estimated to be $\kappa = \kappa_{\text{MD}} \frac{dT_{\text{MD}}}{dT}$. In this work, all quantum corrections were made based on the experimental value of Debye temperature (=645 K). The correction factor derived from the Debye temperature for the Tersoff potential[38] would be different to a certain degree; however, the quantum correction based on the experimental value should be sufficient for assessment of the defect size and concentration effect on the thermal conductivity as the same correction factor is applied to all simulation results.

(d) Cell size dependence of k. In the direct method, the predicted thermal conductivity is a function of simulation cell length. If the axial length of the simulation cell is not sufficiently longer than the mean free path of phonons in the system, phonon scattering in the heat sink and heat source regions may inhibit thermal conduction and consequently lower thermal conductivity.[35,36] The finite-size effect is often unavoidable if a finite-size simulation cell is employed in determination of bulk thermal conductivities. This dependency can be removed by extrapolating the simulation results with various finite-size cells to the infinite system. According to Schelling *et al.*,[39] the relationship between size-dependent thermal conductivity and simulation cell length ($L_{\text{tot}} = 2L_z$, where L_z is the distance between the heat source and heat sink centers, which is half of the total simulation cell length) is given by $\frac{1}{\kappa} \propto (\frac{1}{l_\infty} + \frac{2}{L_z})$, where l_∞ is the phone mean free path for the infinite system. From linear extrapolation with a set of calculated $(1/L_z, 1/\kappa)$ values to $1/L_z = 0$, we can approximate the bulk thermal conductivity.

This method, on the basis of Matthiessen's rule, assumes that the inverse of the effective phonon mean free path (l_{eff}) can be obtained by adding the inverses of the bulk phonon mean free path (l_{eff}) and the boundary scattering contribution (in a finite system), i.e., $\frac{1}{l_{\text{eff}}} = \frac{1}{l_\infty} + \frac{2}{L_z}$. The factor of 2 in the boundary scattering term accounts for the mean scattering distance of phonons traveling from the heat source to the heat sink. According to the simple kinetic theory, $\kappa = \frac{1}{3} C_v v l$, where C_v is the specific heat per unit volume, v is the group velocity, and l is the mean free path, the thermal resistivity ($1/k$) is given by

$$\frac{1}{\kappa} = \left(\frac{1}{\kappa_\infty} + \frac{\alpha}{L_z} \right), \quad (2)$$

where α is a size-independent constant ($= 6/C_v v$).

For the composite simulation cell employed in this work, the overall thermal resistivity equals the length-weighted average resistivity, $\kappa_{\text{eff}}^{-1} = [(2L_B + L_S)/L_z] \kappa_B^{-1} + (L_I/L_z) \kappa_I^{-1}$, from $J = -\kappa_{\text{eff}} \frac{\Delta T}{L_z} = -\kappa_S \frac{\Delta T_S}{L_S} = -\kappa_B \frac{\Delta T_B}{L_B} = -\kappa_I \frac{\Delta T_I}{L_I}$, where $\Delta T = \Delta T_S + \Delta T_B + \Delta T_I$ and $\kappa_S = \kappa_B$. The effective conductivity is rewritten as

$$\kappa_e = \frac{\kappa_B \kappa_I}{\kappa_I \delta_B + \kappa_B \delta_I}, \quad (3)$$

where $\delta_B = (2L_B + L_S)/L_z$ and $\delta_I = L_I/L_z = 1 - \delta_B$. Substituting Eq. (3) into Eq. (2), we obtain

$$\frac{1}{\kappa_{\text{eff}}} = \frac{1}{\kappa_B} \delta_B + \frac{1}{\kappa_I} \delta_I = \left(\frac{1}{\kappa_\infty} + \frac{\alpha}{2L_B + L_S + L_I} \right). \quad (4)$$

If $L_I \gg 2L_B + L_S$ (or $\delta_B \approx 0$ and $\delta_I \approx 1$), the thermal conductivity of the composite cell (k_{eff}) can be assumed to be equal to that of the vacancy-embedded matrix (k_I). Thus, we can evaluate the contribution of phonon-vacancy scattering to bulk thermal conductivity by extrapolating a corresponding $1/k_{eff}$ vs $1/L_z$ plot to $L_z \to \infty$ (or $1/L_z \to 0$).

III. RESULTS AND DISCUSSION

For reference sake, first we calculated κ for bulk c-Si at 300 K by extrapolating the simulation results with various finite-size cells to the infinite system. Because the defect-free c-Si system has higher κ (i.e., a smaller intercept in the $1/\kappa$ vs $1/L_z$ plot) than other defected systems, a relatively longer simulation cell is needed for more precise extrapolation. Within the composite cell scheme, the intermediate layer thickness (L_I) was varied from 21.7252, 43.4504, 65.1756, and 86.9008 to 130.3512 nm (corresponding to 40, 80, 120, 160, and 240 units, respectively, in the ⟨100⟩ direction), while the thicknesses of the heat source (and heat sink) and buffer layers were fixed at $L_S = 5.4313$ Å and $L_B = 54.313$ Å, respectively.

The insets of Fig. 3 show two examples of the temperature profiles from the longest and shortest simulation cells, which clearly demonstrate that the temperature profiles in the intermediate layers (hatched) are well fitted to linear functions while they are virtually symmetric about the center of the heat source (or sink) layer. This advocates that heat conduction in the intermediate layers obeys Fourier's law with no significant interference from the heat source and heat sink, and it also occurs symmetrically in the simulation domain.

In Fig. 3, calculated $1/\kappa$ values are plotted as a function of $1/L_z$, exhibiting a linear pattern. From a standard least-squares linear regression, the slope and intercept of
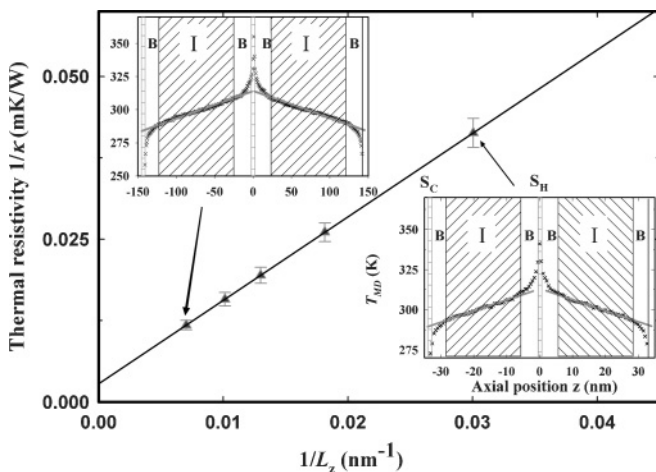

FIG. 3. Thermal resistivity ($1/\kappa$, with quantum correction) for defect-free Si as a function of simulation cell length at 300 K. L_z is the distance between the centers of the heat source and sink layers, which is half of the total simulation cell length (L_{tot}). Insets show MD temperature (T_{MD}) profiles as a function of axial position (z) from the longest and shortest simulation cells, exhibiting linear temperature gradients in the intermediate layers (hatched), as represented by thin solid lines. In the insets, S_H, S_C, B, and I indicate the heat source, heat sink, buffer, and intermediate layers, respectively.

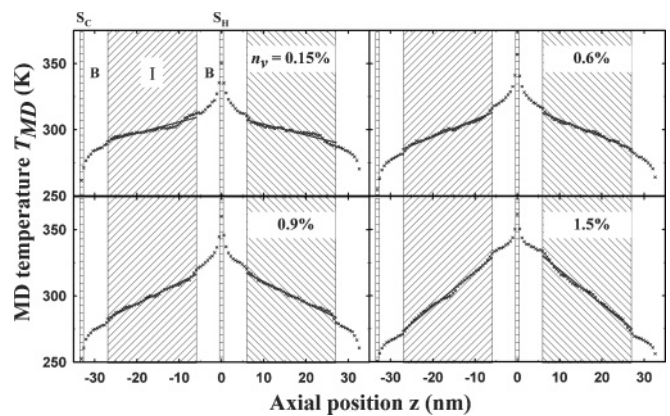FIG. 4. MD temperature (T_{MD}) profiles sampled from the V_{12}-embedded defective systems of four different vacancy concentrations, $n_v = 0.15\%$, 0.6%, 0.9%, and 1.5%. Data are from the simulation cell consisting of $10 \times 10 \times 122$ units (corresponding to $3.8405 \times 3.8405 \times 65.1756$ nm³) and the sample temperature of 300 K. All profiles exhibit linear temperature gradients in the intermediate layers (hatched), as represented by thin solid lines. S_H, S_C, B, and I indicate the heat source, heat sink, buffer, and intermediate layers, respectively.

the $1/\kappa$ vs $1/L_z$ plot are estimated to be 2.56×10^{-9} m² K/W and 0.0028 mK/W, respectively. From the intercept, the κ is predicted to be 235.71 ± 7.53 W m⁻¹ K⁻¹ (before quantum correction $= 357.14 \pm 11.41$ W m⁻¹ K⁻¹) considerably overestimated compared with the experimental value of 156 W m⁻¹ K⁻¹ (Ref. [40]). This discrepancy could be attributed to the tendency of the Tersoff potential to describe the Si structure somewhat rigid.[16] Taking the slope and intercept values, we also estimated the bulk phonon mean free path by $l_\infty = [\text{slope}]/[2 \times \text{intercept}]$; the predicted value of 228.991 ± 10.521 nm is comparable to 300 nm as experimentally estimated.[41,42]

Next, we examined how the presence of vacancy defects affects thermal conductivity. For each defect type, we considered four different vacancy concentrations ($n_v = 0.15\%$, 0.6%, 0.9%, and 1.5%). Figure 4 shows selected time-averaged temperature profiles that were used to compute κ for V_{12} at $n_v = 0.15\%$, 0.6%, 0.9%, and 1.5%. All of the temperature profiles are fitted by linear functions (represented by solid lines) in the vacancy-embedded intermediate layers, although strong nonlinear profiles are shown in the buffer layers, particularly near the heat source and heat sink layers. This confirms that the defective regions are not affected by the unphysical scattering associated with velocity swapping.

Figure 5 shows predicted κ values as a function of vacancy concentration for V_4, V_6, and V_{12}. As n_v increases, κ rapidly decreases; the presence of 1.5% vacancies leads to a 95% reduction in κ (13.20 ± 0.33, 10.65 ± 0.23, and 10.60 ± 0.20 W m⁻¹ K⁻¹ for the V_{12}, V_6, and V_4 cases, respectively), as compared to the defect-free c-Si (235.71 ± 7.53 W m⁻¹ K⁻¹). Even for $n_v = 0.15\%$, phonon transport tends to be significantly impeded as κ drops by over 60% (175.35 ± 24.2, 98.99 ± 8.17, and 87.42 ± 9.84 W m⁻¹ K⁻¹ for the V_{12}, V_6, and V_4 cases). Note that at $n_v = 0.15\%$ there are only two V_{12}, four V_6, or six V_4 clusters in the $10 \times 10 \times 40$ simulation cell (16000 atoms). The large standard deviation of κ at low-vacancy
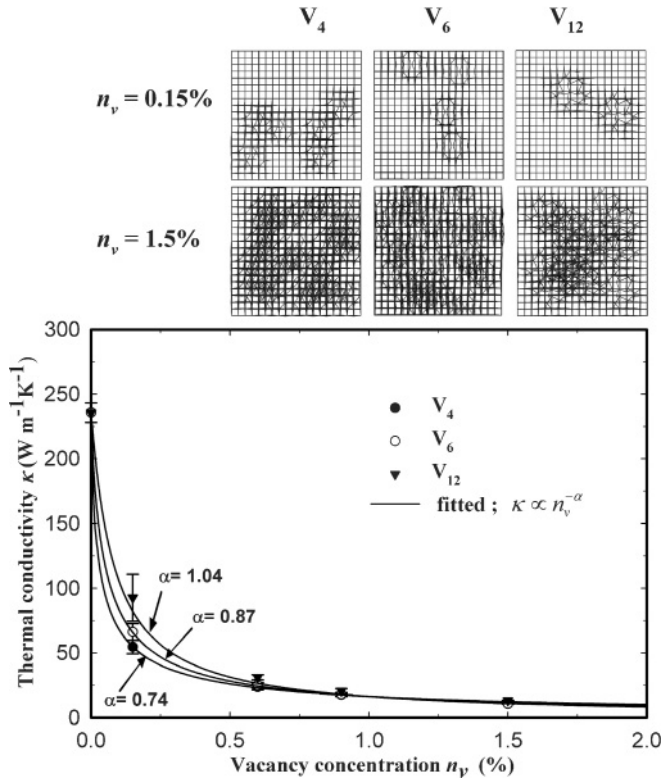
FIG. 5. Calculated bulk thermal conductivities at 300 K (with quantum correction) as a function of vacancy concentration for the V_4-, V_6-, and V_{12}-embedded Si systems. In the upper panels, selected cross-section wireframe views along the heat flow (or $\langle 100 \rangle$) direction are also shown for two different vacancy concentrations.

concentrations (especially when $n_v = 0.15\%$) is due to the fact that the heat transfer from the source to the sink is strongly affected by the location of vacancy clusters. As the number of clusters increases, the standard deviation decreases with a well-converged κ value.

Figure 5 also shows a nonlinear decay of κ with n_v. The calculated values are well fitted with an inverse power-law relation, $\kappa \propto n_v^{-\alpha}$, with $\alpha = 1.04$, 0.87, and 0.74, respectively, for the V_{12}, V_6, and V_4 cases. The nonlinear relation between κ and n_v has also been reported for carbon materials such as carbon nanotubes[19] and diamond.[20] The exponent α is a measure of how rapidly κ drops with increasing n_v; that is, a smaller exponent implies a steeper decrease of κ. According to our results, smaller clusters would more effectively inhibit phonon transport for the same vacancy concentration.

It is worth noting that the reduction of κ with n_v is a function of cluster size particularly when n_v is low. To understand the correlation between phone scattering and cluster size, we approximated the rate of phonon-vacancy scattering in the vacancy-embedded region; here, the rate of phonon scattering due to vacancy aggregates is, according to previous studies,[27,43] given by $\tau^{-1} = cn\pi d_e^2/4$, where c is the phonon group velocity, n is the number density of vacancy clusters, and d_e is the effective diameter assuming each cluster has a spherical shape. Suppose c is insignificantly affected by cluster size, the normalized scattering rate for V_6 or V_{12} with respect to V_4 can be approximated by $\gamma_{V_N} = \tau_{V_N}^{-1}/\tau_{V_4}^{-1} = n_{V_N} d_{e,V_n}^2 / n_{V_4} d_{e,V_4}^2$ ($N = 6$ or 12). Here, the

effective diameters were estimated based on defect-induced strain fields. For each vacancy cluster, we first counted the number of strained Si atoms that have strain energy higher than a given cutoff value, and then calculated the volume of a corresponding sphere which can accommodate the strained and vacant atoms in the c-Si lattice. With the volume, the corresponding effective diameter was calculated by $d_e = (6V/\pi)^{1/3}$. For cutoff strain energies of 0.02–0.2 eV, the effective diameters are roughly estimated to be 13.35–7.72 Å, 15.02–8.14 Å, and 17.01–8.70 Å for V_4, V_6, and V_{12}, respectively. Taking the average values of the diameters (as the energy cutoff is rather arbitrary), γ_{V_6} and $\gamma_{V_{12}}$ are approximated to be 0.75 ± 0.05 and 0.59 ± 0.09, respectively, at $n_v = 0.15\%$. The increase of scattering rate with decreasing cluster size unequivocally supports our simulation results showing that a smaller cluster size leads to a more rapid reduction in κ for the same vacancy concentration. We admit that this approach would be oversimplified, but should be physically sound and sufficient for approximation of the scattering rate variation with cluster size, considering that phonon scattering is, to a large extent, determined by defect-induced lattice distortions. The cluster-size dependence of κ becomes insignificant as the density of vacancy clusters increases. When $n_v = 1.5\%$, κ is virtually no longer a function of cluster size. This is likely related to the fact that the projected areas of clusters in the heat-flow direction largely overlap and nearly cover the heat-flow cross section, as illustrated in Fig. 4. Note that phonons travel in straight lines from the source to the sink; the transport of most of the phonons could be blocked if the cross section is covered by vacancy clusters, and thus phonon transport becomes rather insensitive to the cluster size.

Finally, we estimated how the phonon mean free path is affected by vacancy concentration and cluster size. Figure 6 shows the normalized phonon mean free paths for various vacancy-embedded systems with respect to the bulk value ($\lambda = l/l_{c-Si}$). The normalized mean free paths rapidly decrease with n_v; at $n_v = 1.5\%$ the predicted values are 0.1202 ± 0.0046, 0.0913 ± 0.0039, and 0.0846 ± 0.0038 for the V_{12}, V_6, and V_4 cases, respectively. Similar to the thermal conductivity
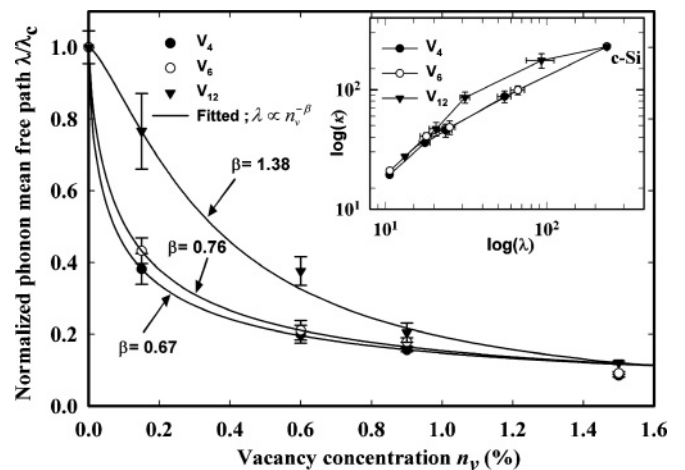

FIG. 6. Calculated phonon mean free paths at 300 K as a function of vacancy concentration for the V_4-, V_6-, and V_{12}-embedded Si systems. Inset shows a correlation between thermal conductivity and phonon mean free path; both κ and l rapidly decrease with n_v.

variation (see Fig. 4), the results are also well fitted to an inverse power-law relation, $l \propto n_v^{-\beta}$, with $\beta = 0.67$, 0.76, and 1.38 for the V_4, V_6, and V_{12} cases, respectively. In addition, the inset clearly shows that there is a direct correlation between thermal conductivity and phonon mean free path, consistent with the kinetic theory ($\kappa \propto l$). In undoped (or lightly doped) semiconductors, heat is transported primarily by lattice vibrations (phonons) at moderate temperatures (where the effect of radiation is negligible).[44] Likewise, electronic and radiative contributions can be ignored in the c-Si system considered; therefore, the mean free path of phonons is an important indicator regarding how effectively thermal energy is carried through the model Si structures.

IV. SUMMARY

Nonequilibrium molecular dynamics simulations based on the Tersoff potential were performed to examine the effect of vacancy defects on the thermal conductivity (κ) of c-Si. For reference sake, we first calculated κ for bulk c-Si at 300 K by extrapolating the simulation results with various finite-size cells to the infinite system; the predicted κ is 235.71 ± 7.53 W m^{-1} K^{-1} (before quantum correction $= 357.14 \pm 11.41$ W m^{-1} K^{-1}), which tends to be overestimated compared with the experimental value of 156 W m^{-1} K^{-1}. κ rapidly decreases with increasing vacancy concentration (n_v) with an inverse power-law relation ($\kappa \propto n_v^{-\alpha}$); the fitted α values are 1.04, 0.87, and 0.74, respectively, for the V_{12}, V_6, and V_4 cases. According to the results, κ drops

to 13.20 ± 0.33 (175.35 ± 24.2), 10.65 ± 0.23 (98.99 ± 8.17), and 10.60 ± 0.20 (87.42 ± 9.84) W m^{-1} K^{-1} in the presence of fourfold V_{12}, V_6, and V_4 clusters, respectively, at $n_v = 1.5\%$ (0.15%). Our calculations also suggest that the reduction of κ with n_v is a function of cluster size particularly when n_v is low; smaller clusters tend to more effectively inhibit phonon transport for the same vacancy concentration. We attempt to explain the cluster-size dependence based on effective cluster diameters for phonon scattering, which were estimated from defect-induced strain fields. When n_v is much greater than 1%, we also find that κ is virtually no longer a function of cluster size because the projected areas of clusters in the heat-flow direction overlap and fully cover the heat-flow cross section. Phonon mean free paths were also estimated by varying vacancy concentration and cluster size; the results are fitted to an inverse power-law relation, $l \propto n_v^{-\beta}$, with $\beta = 0.67$, 0.76, and 1.38 for the V_4, V_6, and V_{12} cases, respectively. Our results also reinforce that the thermal conductivity is directly proportional to the phonon mean free path ($\kappa \propto l$). The improved understanding could offer insight into how to enhance the thermoelectric properties of Si-based materials by defect engineering.

*Author to whom correspondence should be addressed: gshwang@che.utexas.edu

[1] A. I. Hochbaum, R. Chen, R. D. Delgado, W. Liang, E. C. Garnett, M. Najarian, A. Majumdar, and P. Yang, Nature (London) **451**, 163 (2008).

[2] A. I. Boukai, Y. Bunimovich, J. Tahir-Kehli, and J. R. Heath, Nature (London) **451**, 168 (2008).

[3] G. F. Snyder and E. S. Toberer, Nat. Mater. **7**, 105 (2008).

[4] Z. Shao, S. M. Haile, J. Ahn, P. D. Ronney, Z. Zhan, and S. A. Barnett, Nature (London) **435**, 795 (2005).

[5] Y. Nakayama, P. J. Pauzauskie, A. Radenovic, R. M. Onorato, R. J. Saykally, J. Liphardt, and P. Yang, Nature (London) **447**, 1098 (2007).

[6] Y. Cui and C. M. Lieber, Science **291**, 851 (2001).

[7] M. J. Biercuk, M. C. Llaguno, M. Radosavljevic, J. K. Hyun, and A. T. Johnson, Appl. Phys. Lett. **80**, 2767 (2002).

[8] *CRC Handbook of Thermoelectrics*, edited by D. M. Rowe (CRC, Boca Raton, FL, 1995).

[9] A. Majumdar, Science **303**, 777 (2004).

[10] R. Venkatasubramanian, E. Siivola, T. Colpitts, and B. O'Quinn, Nature (London) **413**, 597 (2001).

[11] J. P. Heremans, V. Jovovic, E. S. Toberer, A. Saramat, K. Kurosaki, A. Charoenphakdee, S. Yamanaka, and G. J. Snyder, Science **321**, 554 (2008).

[12] P. F. P Poudeu, J. D'Angelo, A. D. Downey, J. L. Short, T. P. Hogan, and M. G. Kanatzidis, Angew. Chem., Int. Ed. **45**, 3835 (2006).

[13] L. Weber and E. Gmelin, Appl. Phys. A **53**, 136 (1991).

[14] D. Donadio and G. A. Galli, Phys. Rev. Lett. **102**, 195901 (2009).

[15] J.-H. Lee, G. A. Galli, and J. C. Grossman, Nano Lett. **8**, 3750 (2008).

[16] J.-H. Lee, J. C. Grossman, J. Reed, and G. A. Galli, Appl. Phys. Lett. **91**, 223110 (2007).

[17] J. Che, T. Cagin, and W. A. Goddard III, Nanotechnology **11**, 65 (2000).

[18] J. Che, T. Cagin, W. Deng, and W. A. Goddard III, J. Chem. Phys. **113**, 6888 (2000).

[19] D. T. Morelli, Phys. Rev. B **44**, 5453 (1991).

[20] P. G. Klemens and D. F. Pedraza, Carbon **32**, 735 (1994).

[21] T. Yamamoto and K. Watanabe, Phys. Rev. Lett. **96**, 255503 (2006).

[22] S. Coffa and S. Libertino, Appl. Phys. Lett. **73**, 3369 (1998).

[23] G. S. Hwang and W. A. Goddard III, Phys. Rev. B **65**, 233205 (2002), and references therein.

[24] S. Lee, and G. S. Hwang, Phys. Rev. B **78**, 125310 (2008).

[25] S. Lee, R. J. Bondi, and G. S. Hwang, Phys. Rev. B **80**, 245209 (2009).

[26] J. W. Schwartz and C. T. Walker, Phys. Rev. **155**, 969 (1967).

[27] F. Muller-Plathe, J. Chem. Phys. **106**, 6082 (1997).

[28] P. Jund and R. Jullien, Phys. Rev. B **59**, 13707 (1999).

[29] S. S. Mahajan, G. Subbarayan, and B. G. Sammakia, Phys. Rev. E **76**, 056701 (2007).

[30] M. S. Green, J. Chem. Phys. **22**, 398 (1954).

[31] S. G. Volz and G. Chen, Phys. Rev. B **61**, 2651 (2000).

[32] H. B. Callen and T. A. Welton, Phys. Rev. **83**, 34 (1951).

[33] J. Tersoff, Phys. Rev. B **39**, 5566 (1989).

[34]S. Plimpton, J. Comput. Phys. **117**, 1 (1995).

[35]C. Oligschleger and J. C. Schon, Phys. Rev. B **59**, 4125 (1999).

[36]A. Maiti, G. D. Mahan, and S. T. Pantelides, Solid State Commun. **102**, 517 (1997).

[37]C. Kittel, *Introduction to Solid State Physics*, 7th ed. (Wiley, New York, 2006).

[38]H. Wang, W. Chu, H. Jin, and Y. Xiong, Chem. Phys. **344**, 299 (2008).

[39]P. K. Schelling, S. R. Phillpot, and P. Keblinski, Phys. Rev. B **65**, 144306 (2002).

[40]C. J. Glassbrenner and G. A. Slack, Phys. Rev. **134**, A1058 (1964).

[41]Y. S. Ju and K. E. Goodson, Appl. Phys. Lett. **74**, 3005 (1999).

[42]P. G. Sverdrup, Y. S. Ju, and K. E. Goodson, ASME J. Heat Transfer **123**, 130 (2001).

[43]S. Barman and G. P. Srivastava, Phys. Rev. B **73**, 073301 (2006).

[44]J. M. Ziman, *Electrons and Phonons* (Oxford University Press, Oxford, U.K., 2006).